A multichannel feature-based approach for longitudinal lung CT registration in the presence of radiation induced lung damage

1 TITLE PAGE

2

3 Title:

4 A Multichannel Feature-based Approach for Longitudinal Lung CT Registration in the Presence of

5 Radiation Induced Lung Damage

6

7 Authors:

8 A Stavropoulou[1]*, A Szmul[1], E Chandy[1,2], C Veiga[1], D Landau[2,3,] J R McClelland[1]

9 (1) Centre for Medical Image Computing, Department of Medical Physics and Biomedical Engineering,

10 University College London, UK, (2) University College Hospital London, UK, (3) Guys & St Thomas

11 NHS Foundation Trust, UK

12

13 Key Words:

14 radiation-induced lung damage, lung cancer, radiotherapy, computed tomography, longitudinal image

15 registration

16

17

18

19

20

21

22

23

24

25

26

27

28

29

30

31

32

33

34

35

ABSTRACT

Quantifying parenchymal tissue changes in the lungs is imperative in furthering the study of radiation induced lung damage (RILD). Registering lung images from different time-points is a key step of this process. Traditional intensity-based registration approaches fail this task due to the considerable anatomical changes that occur between timepoints. This work proposes a novel method to successfully register longitudinal pre- and post-radiotherapy (RT) lung CT scans that exhibit large changes due to RILD, by extracting consistent anatomical features from CT (lung boundaries, main airways, vessels) and using these features to optimise the registrations.

Pre-RT and 12-month post-RT CT pairs from fifteen lung cancer patients were used for this study, all with varying degrees of RILD, ranging from mild parenchymal change to extensive consolidation and collapse. For each CT, signed distance transforms from segmentations of the lungs and main airways were generated, and the Frangi vesselness map was calculated. These were concatenated into multi-channel images and diffeomorphic multichannel registration was performed for each image pair using NiftyReg. Traditional intensity-based registrations were also performed for comparison purposes. For the evaluation, the pre- and post-registration landmark distance was calculated for all patients, using an average of 44 manually identified landmark pairs per patient. The mean (standard deviation) distance for all datasets decreased from 15.95 (8.09) mm pre-registration to 4.56 (5.70) mm post-registration, compared to 7.90 (8.97) mm for the intensity-based registrations. Qualitative improvements in image alignment were observed for all patient datasets. For four representative subjects, registrations were performed for 3 additional follow-up timepoints up to 48-months post-RT and similar accuracy was achieved.

We have demonstrated that our novel multichannel registration method can successfully align longitudinal scans from RILD patients in the presence of large anatomical changes such as consolidation and atelectasis, outperforming the traditional registration approach both quantitatively and through thorough visual inspection.

MANUSCRIPT MAIN BODY

1. Introduction

Non-small cell lung cancer (NSCLC) is one of the most common cancers in the UK. Historically, the prognosis for lung cancer patients has been poor, but advancements in treatments have caused mortality to decline (Howlander et al. 2020). However, survivors of NSCLC can experience poor quality of life due to the toxicity of radiotherapy (RT) (Marks et al. 2000, Lopez Guerra et al. 2012, Fan et al. 2001). The study of the negative long-term effects of radiation is becoming ever more important as patient survival rates increase. Radiation received during radiotherapy can lead to radiation induced lung damage (RILD). RILD is a time-dependent process, often split into two phases. Acute RILD or pneumonitis, is a phase of inflammation which occurs a few weeks or months after RT and is reversible. Chronic damage (pulmonary fibrosis) is the permanent scarring of the lung tissue that leads to impairment of oxygen transfer (Mehta et al. 2005).

RILD can manifest as anatomical changes in the thoracic cavity such as consolidation, collapse and pleural effusion and can be detected in computed tomography (CT) images as changes in shape, density, texture and position between scans at different time points post-RT (Veiga et al. 2020, Choi et al. 2004, Ikezoe et al. 1988). It is routine clinical practice for RT patients to be scanned every 3-6 months for up to 5 years after treatment. Studying the time-evolution of the radiological changes in these post-RT scans can provide a better understanding of RILD and potentially provide insight in the relationship between RT dose and clinical outcomes (Rosen et al. 2001, Ma et al. 2009, Simone 2017).

Existing scoring systems of RILD are limited, and there is yet no accepted methodology to quantify and measure RILD. Work has previously been done by our group to study global changes in the lungs (Veiga et al. 2018, 2019). Objective image-based biomarkers were developed to quantify and evaluate such global changes as normal lung volume shrinkage, changes in lung shape, distortions of the diaphragm, etc. To calculate these biomarkers, it is only necessary to rigidly align the CT scans from different timepoints pre- and post-RT. Recently, we have been extending our suite of biomarkers to study-local parenchymal tissue changes occurring due to RILD. However, to analyse the temporal evolution of the parenchymal changes it is necessary to align corresponding regions of the lungs. Due to the large anatomical distortions that can occur, accurate alignment cannot be achieved by simple rigid or affine registrations. Deformable image registration can potentially be used to align the image from different time points, but the large anatomical distortions and considerable changes to the appearance of the images due to RILD make these registrations extremely challenging.

1 Traditional intensity-based DIR algorithms align the images based on the similarity of the intensity
2 information in the images. However, the radiological appearance of healthy lung tissue is very different
3 to that of damaged tissue and therefore it is unlikely that accurate alignment can be achieved using this
4 intensity information. Furthermore, there can be large anatomical differences between the pre- and post-
5 RT scans, such as tumour regression, tissue collapse, and fibrosis, which all violate the assumption of
6 a one-to-one correspondence between the images made by most registration algorithms and make it
7 difficult to obtain a meaningful alignment between the scans. Even when a one-to-one correspondence
8 does exist, some manifestations of chronic RILD such as consolidation, atelectasis and cavitation can
9 result in extreme geometrical deformations between the CTs. Consequently, attempting to align the pre-
10 RT and the post-RT scans using traditional intensity-based algorithms usually gives unsatisfactory
11 results. Veiga et al. (2016) investigated and outlined many of the challenges in registering longitudinal
12 RILD lung CTs. Additionally, the difficulties in working with clinical data from multiple institutions
13 must also be considered. There can be large differences in image acquisition parameters and setup such
14 as image resolution, field of view, patient setup and use of contrast that lead to differences in the scans
15 that must be accounted for. Finally, even though follow up scans are usually acquired at breath-hold,
16 baseline scans can sometimes be 4D CT scans, adding to the potential variability between time points.

17

18 Intensity-based deformable image registration (DIR) algorithms have previously been used to co-
19 register pre- and post-RT scans. Cunliffe et al. evaluated the accuracy of the Plastimatch
20 (http://plastimatch.org) and the Fraunhofer MEVIS Fast deformable registration algorithms in
21 registering CT scans before and 3 months after RT. They identified 8 out of 24 patients to have moderate
22 to severe radiation induced changes and it was consistently shown that while the MEVIS algorithm
23 performed better across most patients, the presence of RILD increased registration error for both
24 algorithms (from 1.3mm to 2.5mm for MEVIS and from 2.4mm to 4.6mm for Plastimatch, almost 2
25 times the error in both cases). Spijkerman et al. compared the accuracy of a Demons (Thirion 1998,
26 Vercauteren 2009) and Morphons (Wrangsjö 2005) deformable registration algorithm with a rigid
27 registration. Twenty-two NSCLC patient datasets were used, with pairs of pre and 3-month post-RT
28 PET/CT scans. Two patient datasets were excluded due to the presence of atelectasis and pneumonitis
29 in the follow-up scans. For the remaining datasets, while no major differences were observed between
30 the Demons and Morphons algorithm, both showed improvement compared to the rigid registrations
31 alone. Results were split into three groups according to alignment improvement with the major
32 improvement group having a landmark error decrease from 9.5 ± 2.1 mm to 3.8 ± 1.2 mm, the minor
33 improvement group from 5.6 ± 1.3 mm to 4.5 ± 1.1 mm and the insufficient improvement group from
34 13.6 ± 3.2 mm to 8.0 ± 2.2 mm. While there have been several studies attempting pre- to post-RT lung
35 CT registration, registration of scans further than 3 months post-RT is still largely unexplored. This is
36 likely due to the more dramatic changes seen at longer follow up scans as radiological changes continue
37 to progress up to 24-months post treatment (Veiga et al. 2020). Additionally, scans with significant

1 consolidation and atelectasis are consistently excluded from these studies due to the known difficulties

2 they pose to traditional intensity-based medical image registration algorithms.

3

4 More recently, the use of feature-based information along with intensity-based information has been

5 explored as a mean of improving the performance of registration algorithms in aligning lung CTs by

6 Guy et al. (2018). They developed a DIR framework that employs a combination of the lung CTs, lobe

7 segmentations, vesselness measure images and a mass preserving transformation to register longitudinal

8 images in the presence of atelectasis with considerable success. Although scans with presence of

9 atelectasis were purposefully included, the scan pairs were only a few weeks apart (pre- and mid-

10 treatment). Lobe segmentation in moderately damaged lungs is in itself a very challenging task; in

11 severely damaged or collapsed cases it is often impossible.

12

13 To address current challenges in the co-registration of CT scans in the presence of RILD, in this work

14 we have developed a DIR method that aims to enhance and utilise salient features that are mostly

15 unchanged between time points in order to successfully register scans that are 12 months apart. In our

16 approach however, we discard intensity information to remove the impact that non-deformable

17 parenchymal change would have during registration optimisation. This way, we aim to accurately align

18 the consistent anatomical features between time points and hypothesise that the surrounding tissues will

19 be driven into place accordingly. To the best of our knowledge, this is the first time that multichannel,

20 feature-based DIR has been used to successfully align longitudinal lung CTs with extensive radiation

21 induced lung damage.

1
2
3   **2. Methods**

4

5   2A. Data

6   The patient data were derived from the IDEAL CRT trial cohort, a phase 1/2 nonrandomized multicentre

7   trial that enrolled phase I and II NSCLC patients. 120 patients were enrolled to receive isotoxic tumour

8   RT doses between 63 Gy and 73 Gy in 30 daily fractions over 5 or 6 weeks, concurrent with 2 cycles

9   of cisplatin and vinorelbine (Landau et al. 2016). 15 patient datasets from this trial were selected for

10   use in this study, with each patient having a CT scan at baseline (before RT was administered) and 3,

11   6, 12, and 24 months post-RT. These patients were selected so as to be representative of the changes

12   seen over all patients. Most scans were acquired at breath-hold (deep inspiration) with the remaining

13   being 3-dimensional free-breathing CT or average 4DCT. There was both inter- and intra-patient

14   variability in terms of scan acquisition parameters as well as scan resolution. The in-plane scan

15   resolution ranged between 0.61mm x 0.61mm and 0.98mm x 0.98mm and the slice thickness from

16   0.5mm to 5mm.

17

18   The imaging data was visually reviewed, and each patient dataset was placed into one of four categories

19   according to the expected difficulty of registration between the baseline and 12-month follow up scan.

20   The categories corresponded to: 1) low, 2) medium, 3) high, or 4) very high estimated difficulty of

21   registration. Four scans were placed in each of the low, medium and very high estimated difficulty

22   categories and three scans in the high difficulty one. The criteria considered for this scoring were based

23   on the severity of radiological changes present and scan quality, including: the extent and location of

24   consolidation present in the follow up; the presence and extent of pleural changes and/or atelectasis in

25   the follow up; the differences in lung shape and size; the presence of other anatomical changes

26   associated with fibrosis such as tenting of the diaphragm and mediastinal shift; the presence and extent

27   of cavitation in the follow up; the presence and extent of motion artifacts; whether an image was stitched

28   from multiple scans; the difference in resolution between scans; and how difficult it was to visually

     determine correspondence between scans. An example from each category is presented in figure 1.
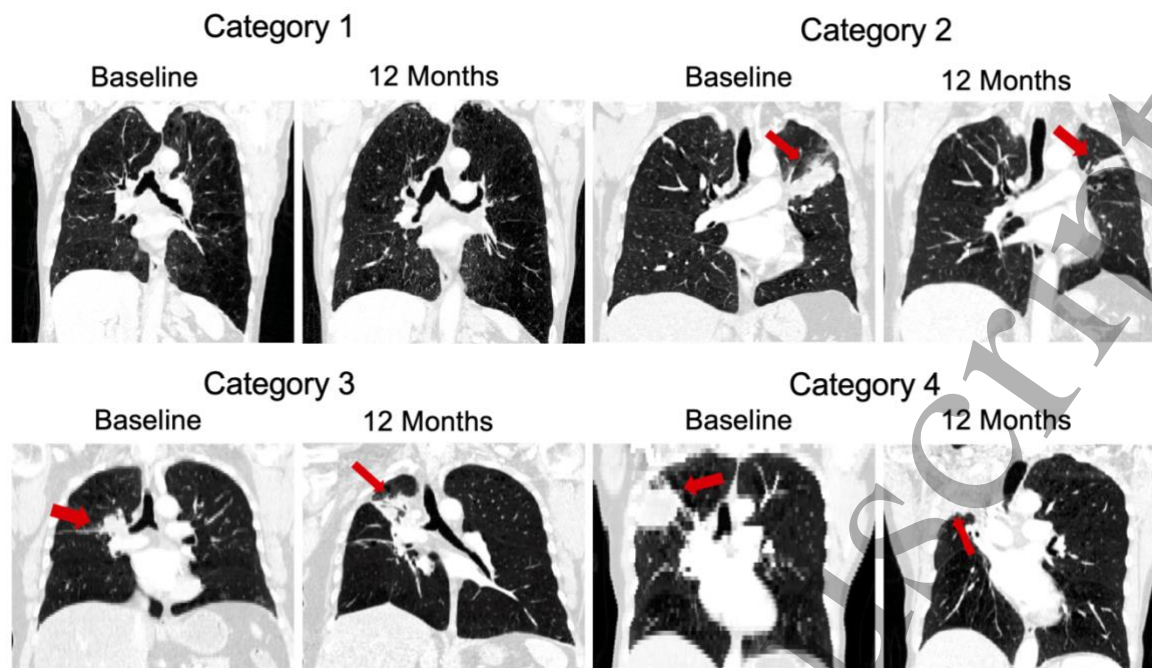
1 **Fig.1.** Baseline and 12-month follow up CT scan pairs of 4 patients with increasing registration

2 difficulty. It can be seen that the scans in category 1 are very similar to each other, with most differences

3 resulting from tumour regression in the left lung and inhalation level of the scans. In category 2, there

4 are noticeable parenchymal and lung volume differences in the ipsilateral lung (left), but mainly

5 contained in the upper lobe where the tumour is located. In category 3 such differences between the

6 scans become more pronounced. Consolidated tissue is present in all 3 ipsilateral (right) lobes of the

7 12-month scan and the damage has extended past the region the tumour originally occupied. There are

8 also changes in the size and shape of the ipsilateral lung between timepoints, with diaphragm tenting

9 present in the follow up scan. In category 4, the most extreme changes are present with the upper right

10 lobe completely collapsed in post-RT. The resolution is very different between the baseline (5mm slice

11 thickness) and follow up (1mm slice thickness) scans, adding to the challenge in the registration.

12

13 2B. Feature representation & pre-processing

14

15 The principal idea behind our approach is to enhance and utilise features that are salient and mostly

16 unchanged between time points while ignoring any information where there may be no clear one-to-

17 one matching that could wrongfully guide the registration. The selected salient features include the lung

18 boundaries, the airways, and the vessel tree.

19

20

21

22

7

1   a.   Lung boundaries & Main airways

2

3 Segmentation of the lungs and the airways were performed semi-automatically as described in Veiga et

4 al. 2018, by using the open-source Pulmonary Toolkit (PTK) (Doel, et al. 2012) to generate automated

5 results. PTK first performs Gaussian smoothing and thresholding on the CT images. Airway

6 segmentation starts with region growing from a point in the trachea and a 26-way connected component

7 approach is applied to organise the airways into a tree-like structure with multiple generations. The

8 segmented airways are removed from the thresholded initial lung masks. The next step separates the

9 lungs into left and right lung, which is initially approached with reversable opening of the lung masks.

10 If that approach is unsuccessful, the watershed method is applied. The final step smooths the separated

11 lungs individually using morphological operations. All segmentations were subsequently manually

12 edited by a radiation oncologist or a medical physicist (EC/CV) using ITK-SNAP (Yushkevich et al.

13 2006).

14

15 Instead of using the binary segmentations directly, we opted to use signed distance transforms derived

16 from the segmentations. Intensity based registrations are driven by the intensity gradient in the images

17 being registered, but for binary segmentations the image gradient is 0 everywhere except directly at the

18 boundary of the segmentations. This can cause problems in cases where the structure is significantly

19 misaligned to start with, as no gradient information is available in the segmentations to drive the

20 structures together. A common approach to combat this, is to smooth the binary images before

21 registration, but this also has the effect of smoothing the segmentation boundary. Therefore, by using

22 signed distance transforms instead, we introduce the necessary gradient while simultaneously enhancing

23 the structure boundary. However, using a Euclidean distance map would cause the registration to align

24 all voxels that are equidistant from the segmentation boundary, regardless of how far they are from that

25 boundary. A more desirable behaviour is to only align voxels near the boundary, with more weight

26 placed on the voxels the closer they are to the boundary. This can be achieved using a distance transform

27 with a steep gradient at the boundary that quickly drops off away from the boundary. Therefore, a

28 distance transform of the form $y = 1 - \frac{1}{1+x}$ was used. The distance transforms were masked out after

29 a distance of 12 voxels from the boundary so that their effect in the registration is nullified once the

30 distance from the structure boundary becomes too large to be relevant. Examples of the distance

31 transforms generated are presented in figure 2.

32

33

34

35

36

1

2   b.   Vessels

3

4   The vesselness measure was used to capture and represent the vessel information. The vesselness

5   measure (Frangi et al. 1998) is a vessel detection approach that uses the Hessian matrix of each voxel

6   to describe the curvature at that voxel. The eigenvalues of the Hessian can indicate if the voxel is part

7   of a blob-like, tube-like, or plate-like structure, and the relative brightness or darkness of the structure

8   compared to the background. Computing these values at multiple scales enables a vesselness value to

9   be calculated for each voxel, which effectively measures how likely it is that the voxel belongs to a

10   vessel. The Pulmonary Toolkit (Doel et al. 2012) was used to calculate the vesselness.

11

12   Once generated, the two distance transforms and the vesselness image were concatenated to form a

13   multi-channel (4D) image, with the lung boundary distance transform in the first channel, the airway

14   boundary distance transform in the second channel, and the vesselness in the third. Examples of the

15   vesselness images generated can be found in figure 2.
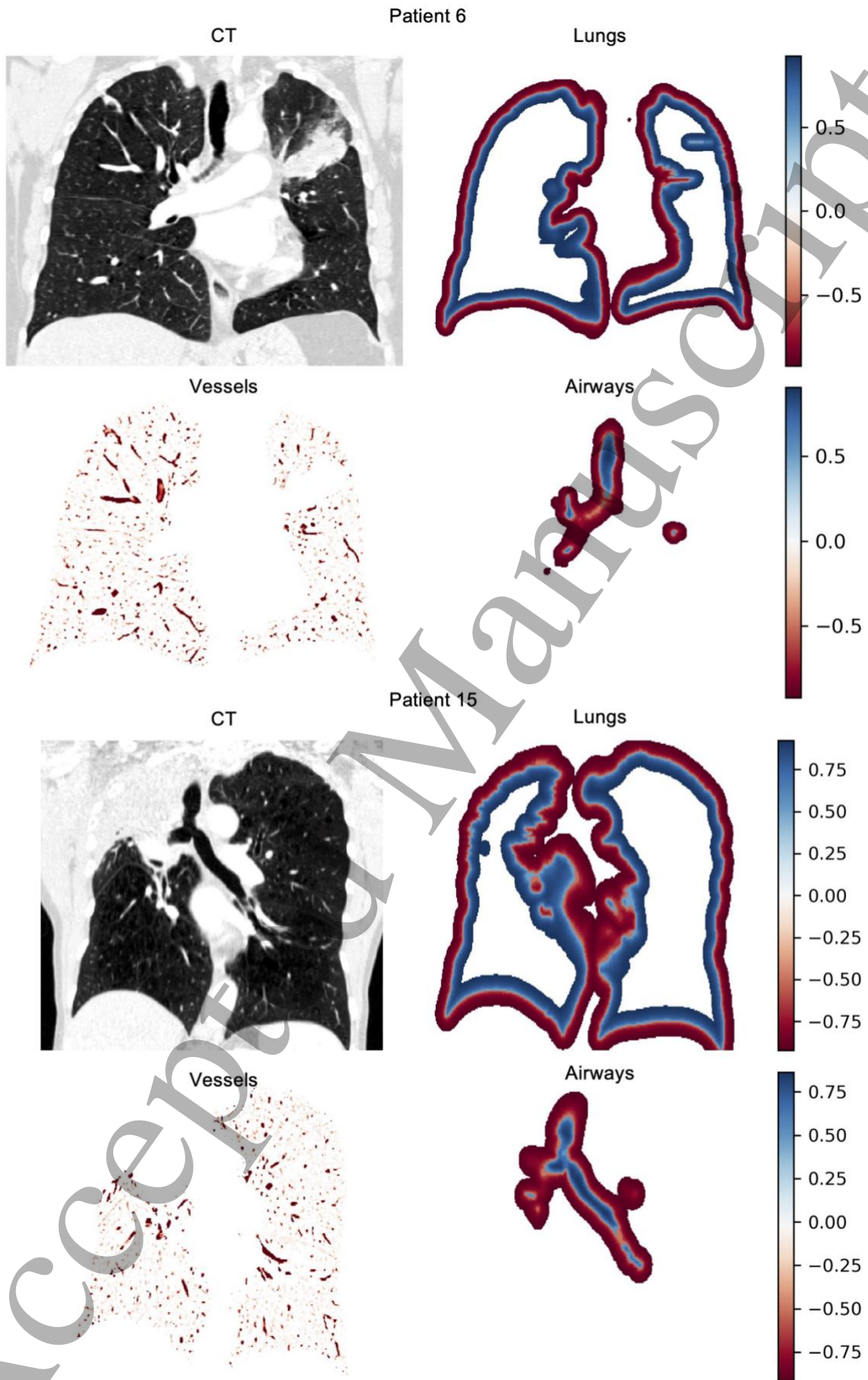
Fig.2. Feature images of patient 6 at baseline (category 2) and patient 15 at 12 months (category 4). From each CT the lung distance transform, airway distance transform and vesselness are extracted. Note that atelectatic tissue (patient 15, upper right lobe) is encompassed in the lung feature image.

2C. Registrations

The CT images were co-registered using the open-source NiftyReg registration software (https://github.com/KCL-BMEIS/niftyreg) which implements a B-spline based free form deformation (FFD) algorithm (Modat, 2010). Good initial alignment of the source and target images is vital for the success of a deformable registration. The images were initially rigidly co-registered using the block-matching algorithm (Ourselin et al. 2001) available in NiftyReg, using a strategy for bone anatomy alignment described in Veiga et al. (2018). Diffeomorphic deformable registrations were then performed using the stationary velocity field parameterisation available in NiftyReg (Modat, 2012).

In NiftyReg, transformations are parameterised by a control point grid. The free form deformation (FFD) algorithm locally deforms the underlying control point grid of the image and interpolates the deformation field using cubic B-splines. The transformation is optimised using a conjugate gradient ascent optimiser. Diffeomorphic registrations have been implemented in NiftyReg using a log-Euclidean FFD approach where a spline model of a stationary velocity field is exponentiated to yield a diffeomorphism. This implementation results in invertible transformations that preserve the topology of the input images. These diffeomorphic transformations are performed symmetrically, with the backwards and forwards transformations being calculated simultaneously.

NiftyReg can perform multi-channel registrations. With multi-channel registrations, each input image (source and target) can consist of multiple channels, each holding complementary information. The similarity between the images is calculated independently for each channel and then summed. Different similarity measures can be used for each channel, and the channel similarities can be weighted relative to each other to control the influence that each channel has on the registration.

Optimisation of the registration parameters was carried out for those parameters that were expected to have the greatest effect on the registration results, namely: choice of image similarity measure and weight for each channel, choice of and weight of the penalty term, and spacing of the B-spline control point grid. Over 50 combinations of parameter values were examined and since each registration required multiple hours to complete, the optimisation was only performed on four representative test cases instead of on the full data set. Similarity measures considered were the SSD (sum of square difference), LNCC (local normalised cross correlation) and NMI (normalised mutual information), with

1 relative weights for each channel ranging from 0.5 to 100. Bending energy and linear energy were
2 considered for the penalty term, but ultimately the linear energy was not used as it penalises stretching
3 and shearing, which are useful deformations for these registrations. The control point grid spacing tested
4 ranged from 1mm to 7mm. The best parameters were chosen after evaluating the registration results
5 visually and quantitatively by landmark registration error (see section 2D for how this was calculated).
6 The results with lowest mean and median landmark error were selected to be closely visually inspected,
7 and the parameters providing the best alignment in the structures of interest while also keeping to
8 plausible deformations were favoured. Overall, it was observed that the registrations were robust to
9 small changes in individual parameter values, therefore the most important aspect of the optimisation
10 was achieving appropriate balance between the terms. It was also observed that changes in the control
11 point grid spacing had a stronger regularising effect than changes in the regularisation term itself.
12 Finally, the best results were given when the vesselness channel was weighed considerably higher than
13 the lungs and airways, due to the large-scale structures being easier to align than the smaller and more
14 detailed vessels. The best parameters were found to be the SSD with a weight of 1 for the lung and
15 airways distance transform channels and the NMI with a weight of 2.5 for the vesselness channel;
16 bending energy with a weight of 0.001 for the penalty term; an isotropic control point spacing of 5mm.
17

18 The optimised parameters were then used to perform pairwise registrations for each of the 15 patient
19 datasets, registering the baseline scan with the 12-month follow up. For 4 out of the 15 patients (one
20 from each category), pairwise registrations were also performed between the baseline and remaining
21 follow up scans (at 3, 6, and 24 months), in order to investigate the effect of temporal distance on
22 registration accuracy.
23

24 2D. Landmark Placement & Landmark Registration Error
25

26 In order to evaluate the registrations corresponding landmarks were manually identified in the images
27 using the NiftyView application (https://github.com/NifTK/NifTK). Landmarks were placed on vessel
28 and airway bifurcations. The landmarks were distributed over both lungs and for all datasets at least
29 half the points were located in the ipsilateral lung, where larger changes were expected. Where possible,
30 landmark points were concentrated close to the tumour (in the baseline) and RILD (in the follow up),
31 as those are the areas of interest that must be assessed. However, in cases where the geometrical changes
32 were substantial and the damage was particularly severe, it was impossible to identify matching
33 landmark pairs in those areas of interest. As manual landmark identification is a time consuming and
34 laborious task, landmarks were identified for all 5 timepoints in only 4 out of the 15 patients (one from
35 each category). For the remaining 11 patients, landmark pairs were identified between the baseline and
36 12-month follow up scan only. An average (range) of 44 (38-65) landmarks were identified per CT. An
37 example of landmark distribution for one dataset is available in figure 3.

1   Quantitative evaluation of the registrations is achieved through calculation of the post-registration

2   landmark distance (D_{reg}). D_{reg} is calculated as the Euclidean distance between the landmark points in

3   the source image and the corresponding landmark points from the target image transformed by the

4   registration result. Since the registrations were symmetrically performed in two directions, D_{reg} was

5   calculated for both registration directions and averaged. For comparison, the pre-registration landmark

6   distance (D_{pre}) was also calculated as the Euclidean distance between the corresponding landmarks in

7   the images without any deformable transformation being applied.
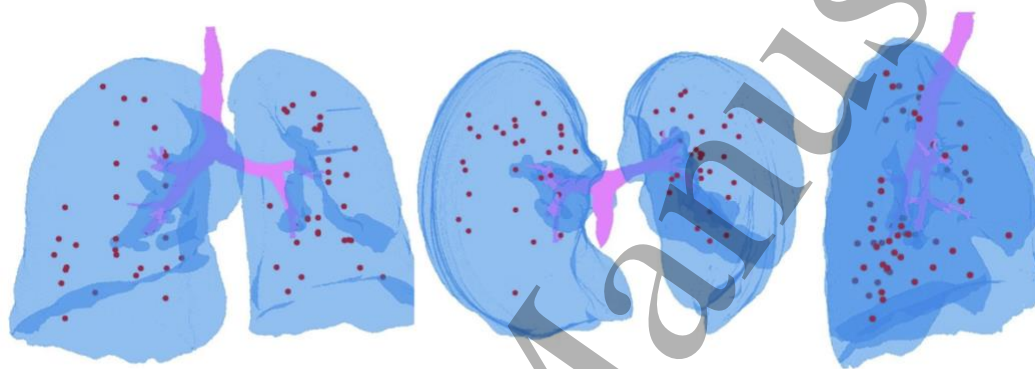
Fig.3. Coronal, axial and sagittal views of a 3D rendering of the baseline lungs and main airways of patient dataset with the landmark points in red.

2E. Intensity only registrations

To demonstrate the differences between the feature-based approach presented in this work and traditional intensity-based approaches, an intensity-based registration was performed for each of the 15 datasets using the 12-month follow up scan. The same diffeomorphic NiftyReg registration algorithm was employed but without the multichannel implementation. The original CT images were used as the inputs and parameters were kept consistent with the parameters of the multichannel registrations where appropriate (e.g., control point spacing, similarity measure (NMI), regularisation).

1   **3. Results**

2

3   3A. Multichannel registrations

4

5   <u>12 months</u>

6   A summary of the numerical results of co-registering pre and 12-months post-RT scans using the

7   proposed multichannel method is reported in table 1. Across all patients, the mean (standard deviation)

8   D_{pre} is 15.95 (8.09) mm, and after deformable registration, D_{reg} decreases to 4.56 (5.70) mm. A clear

9   improvement in the mean and median D_{reg} is noticeable for all 15 patients. For four patients, the mean

10   D_{reg} is smaller than the corresponding mean slice thickness and for nine patients, their mean D_{reg} is less

11   than twice their mean slice thickness. The median D_{reg} is less than the slice thickness for 12 out of 15

12   patients.

13

14

15   **Table 1**. Summary statistics for pre- and post-registration landmark distance

Category	Patient No	No of landmarks	Mean *Slice Thickness* (*mm*)	Mean *Dpre* (*mm*)	Mean *Dreg* (*mm*)	Median *Dpre* (*mm*)	Median *Dreg* (*mm*)	S.D. (*mm*)
1	1	65	1.25	3.68	1.03	3.35	0.84	0.65
	2	50	2.50	14.47	2.77	10.29	1.97	3.41
	3	48	2.75	10.19	1.82	10.26	1.49	1.25
	4	42	1.00	7.50	1.13	4.78	0.68	2.64
2	5	48	3.75	16.97	3.13	13.78	2.05	3.69
	6	42	0.85	14.99	2.80	14.46	0.79	5.46
	7	43	1.25	24.59	7.69	25.23	4.77	8.57
	8	41	2.50	15.54	2.18	16.53	1.39	2.76
3	9	36	5.00	25.57	8.38	22.48	2.44	9.89
	10	38	2.00	20.36	5.97	16.83	1.86	8.08
	11	43	5.00	12.01	6.54	6.27	1.90	10.25
4	12	38	2.10	13.81	6.16	12.23	5.19	4.47
	13	38	1.25	20.45	6.21	17.47	1.47	8.58
	14	45	5.00	16.65	6.34	13.93	1.91	7.81
	15	39	3.00	22.46	6.27	22.46	2.61	8.00

14

1 In figure 4, the distributions of landmark errors before and after the registration are presented for all 4

2 categories. In all cases, a decrease in the median, 25th percentile and 75th percentile distance as well as

3 a narrowing of the distributions can be observed. As expected, in the two easier categories (1 and 2)

4 corresponding to cases with mild or moderate changes, higher registration accuracy was achieved

5 compared to the categories that correspond to cases with more extensive damage (3 and 4), as

6 demonstrated by the lower D_{reg}. The relative improvements between the D_{pre} and D_{reg} are also larger for

7 the lower categories, as can be seen in table 1. It is important to acknowledge the presence of outlier

8 D_{reg} values in these results, with a number of individual D_{reg} over 25mm for categories 2-4, as can be

9 seen in figure 4. These errors are mainly present in the more difficult cases and usually in the ipsilateral

10 lung where damage is present and the deformations to recover are the largest. Figure 5 shows examples

11 of results from each category.

12
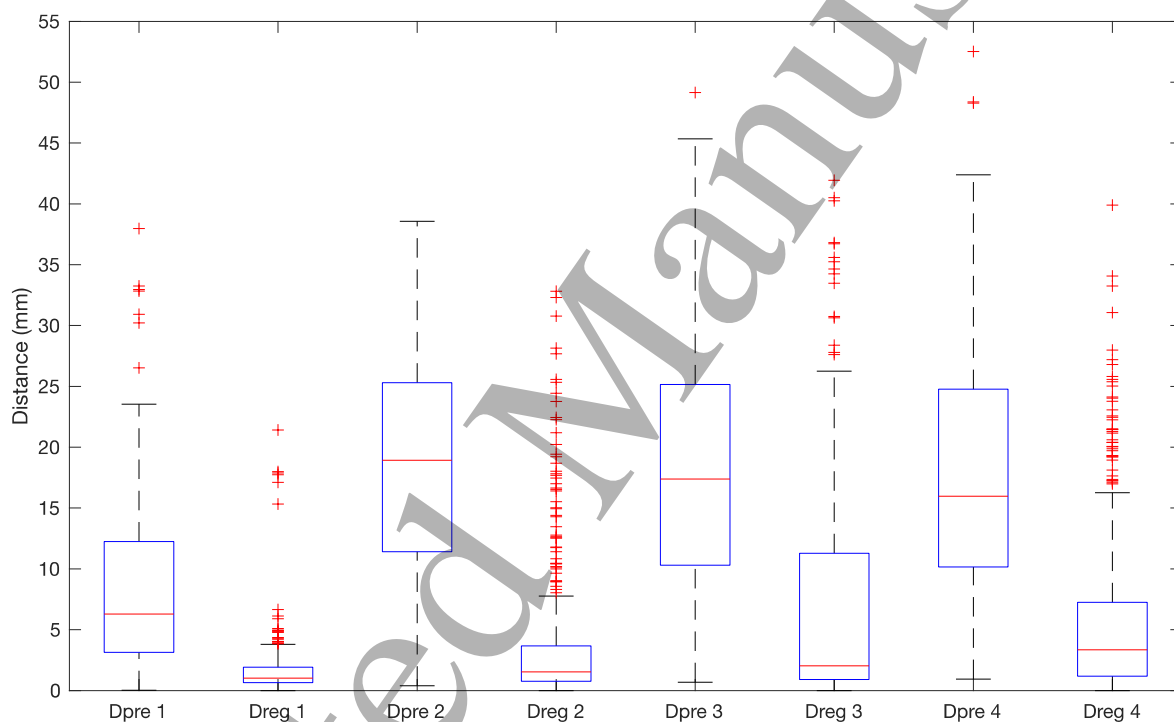
13

14

15 **Fig. 4.** The distribution of D_{pre} and D_{reg} for each data category presented in box plots. The red line

16 represents the median and the bottom and top edges of each box plot represent the 25th and 75th

17 percentiles respectively. The whiskers extend to the most extreme data points that are part of the

18 distribution and the outliers are points beyond ±2.7 std and are plotted with the + symbol.

19

20 When looking at the D_{pre} and D_{reg} for each patient, it becomes apparent that even though some patients

21 have a similar mean D_{pre}, the D_{reg} can vary substantially. For example, patient 2 has a mean D_{pre} of

22 14.47mm and a mean D_{reg} of 2.77mm, but patient 12 has a lower mean D_{pre} of 13.81mm and a mean

23 D_{reg} of 6.16mm, which is more than double that for patient 2. This suggests that D_{pre} may not be the

1 only factor that determines the success of a registration. Other important factors include the type of

2 damage, its location, and how extensive it is. Some cases might have very large D_{pre} but that may be

3 due to global rotations or shearing of the lung tissue. These global changes are easier to align compared

4 to more localised and less well-defined changes such as the appearance of consolidation or atelectasis.

5

6

7 <u>Qualitative observations</u>

8 In addition to the quantitative evaluation performed above, it is vital to visually inspect the registered

9 images in order to gain insight into where and why the registrations failed to align the two scans.

10 Qualitative observations generally agree well with the quantitative results. As expected, the

11 contralateral lung is very well aligned for almost all patient datasets. The largest errors are always

12 located in the ipsilateral lung and usually close to areas of damage, as can be seen in the examples in

13 Figure 5. The lung boundaries are well aligned for all patients, both in the ipsilateral and contralateral

14 lungs, which can be seen in the colour overlays in figure 5. This is especially important in the case of

15 patient 15, where even though the upper right lobe has completely collapsed, the lung boundary is

16 correctly aligned. The main airways are also generally well aligned. The lung boundaries and airways

17 are aligned well even in cases with extreme deformation between scans, such as patient 10 and 15 shown

18 in Figure 5. While the achieved registration results are promising, there are some regions where the

19 alignment could still be improved, especially in cases with extreme deformations. Local misalignment

20 may remain, for example, at smaller airways and vessels, as can be seen in the ipsilateral lungs of

21 patients 10 and 15 (see Figure 5).

22

23 It is important to highlight that the aim of the registrations is not always to make the deformed image

24 look exactly like the target image. For our application, the goal is to align corresponding regions of the

25 images such that the local changes that have occurred between them can then be studied. This is most

26 prominent in examples like patients 10 and 15 in Figure 5, where the scans appear reasonably well

27 aligned and the differences between the deformed scan and target image represent non-deformable

28 changes characteristic of RILD (atelectasis, consolidation) rather than registration errors.

29

30

16

Fig. 5. From left to right: example CTs of patients of increasing difficulty. Top to bottom: Coronal slices from source CT (12 month follow up), target CT (baseline), deformed CT, Colour overlay of target (red) and deformed CT (cyan), landmark points displayed over the deformed CT where the size of the landmark point corresponds to the size of D_{reg} at that point.

1   <u>Serial time-point analysis</u>

2   Temporal evolution of the mean D_{reg} for the four cases of increasing difficulty included in this analysis

3   is presented in figure 6. For three out of the four cases, the landmark error D_{reg} is relatively stable with

4   a general trend to slightly increase over time. This is an expected trend, as the effects of RILD tend to

5   become more pronounced when chronic changes settle in. For patient 15 there is a considerably abrupt

6   increase in D_{reg} at 24 months. The increased error is likely due to the extreme anatomical change present

7   in the 24-month scan, even more so than the 12-month as can be seen in figure 7. These extreme changes

8   also affect the accuracy of the landmark point selection. This higher D_{reg}, therefore, could partially

9   reflect user errors in landmark selection rather than significantly poorer registration accuracy. The

10   lowest errors across all patients are at 3 months, with all of them below 5.5mm and their mean at 3.5mm.

11   Even though this is the time point where radiation pneumonitis appears, its effects seem to have a less

12   negative effect on the registrations compared to the chronic effects of RILD. This is substantiated by

13   Veiga et al. 2020 where it was observed that in the long term, parenchymal change is accompanied by

14   anatomical distortion but at 3 months, less distortion is present.

15
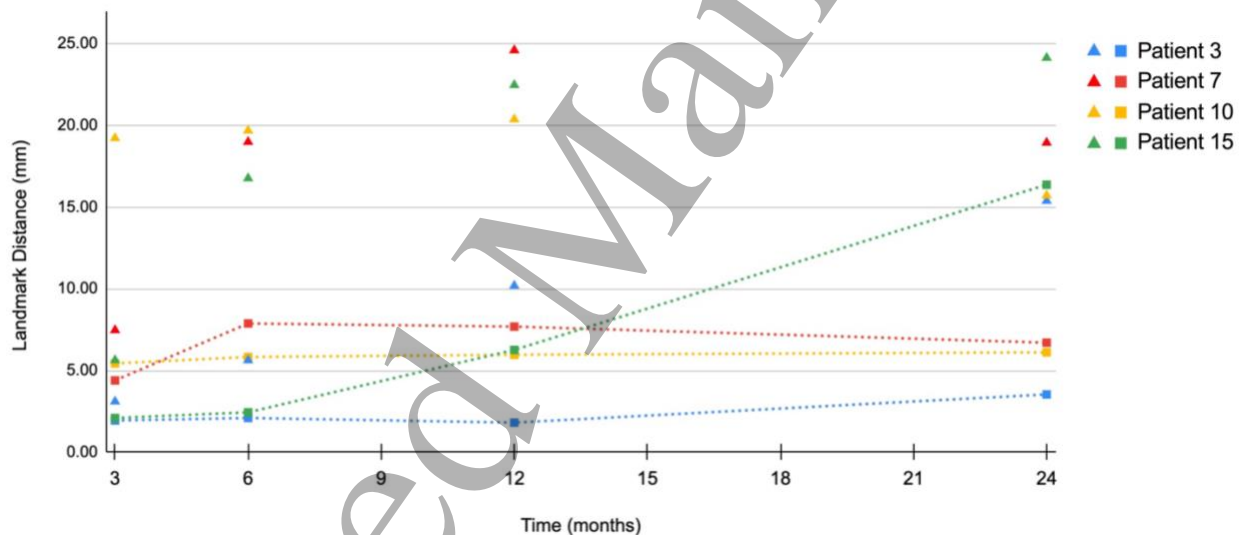
16

17   **Fig. 6.** Mean D_{pre} (triangles) and D_{reg} (squares) for patients 3, 7, 10 and 15 (increasing difficulty) at 3,

18   6, 12, 24 months post-RT
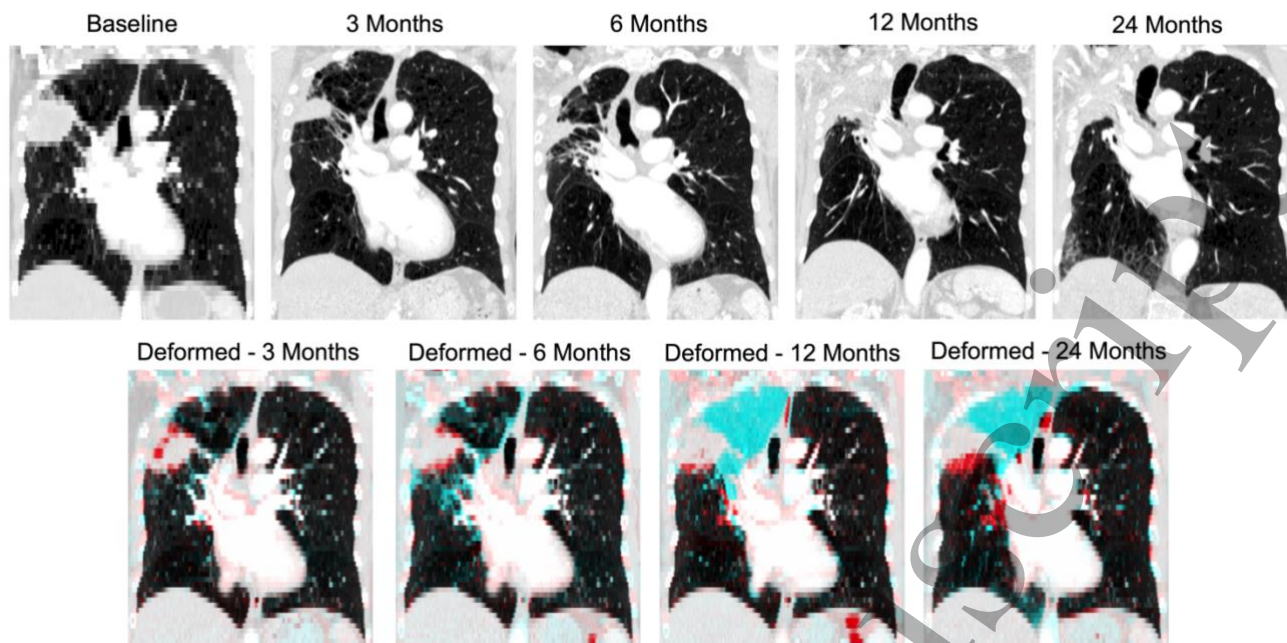
19

20

21

22

23

24

1

Fig. 7. Top row: patient 15 at five time points. Upper right lobe collapse first appears in 12-month scan and remains in the 24-month scan. At 24 months new texture appears in the lower right lobe. Bottom row: Colour overlays between baseline CT and registration results from registering all time points.

3B. Multichannel vs Intensity-based

The overall mean (standard deviation) D_{reg} for the intensity registrations is 7.90 (8.97) mm, which is considerably higher than for the proposed multichannel registrations at 4.56 (5.70) mm. For some cases in categories 1 and 2, where the deformations are smaller and there are no extreme anatomical changes (atelectasis, cavitation, etc.), the intensity approach performs similarly to the proposed multichannel approach, aligning the baseline and 12-month scans well, with D_{reg} close to that of the multichannel registrations. However, that is not the case for the remaining cases with more complex deformations and anatomical changes. The shortcomings of the intensity approach can mainly be seen in the cases where lung tissue or structures expand, contract or change beyond visual recognition, for example where there is collapse or extensive consolidation. An example of this can be seen in the registration result of patient 15 (Figure 8) where in the registration result, the airway in the follow up scan has been extremely stretched to align with the upper right lobe and tumour boundaries of the baseline scan. These deformations are not only anatomically implausible but also fail to align corresponding regions of the lungs.
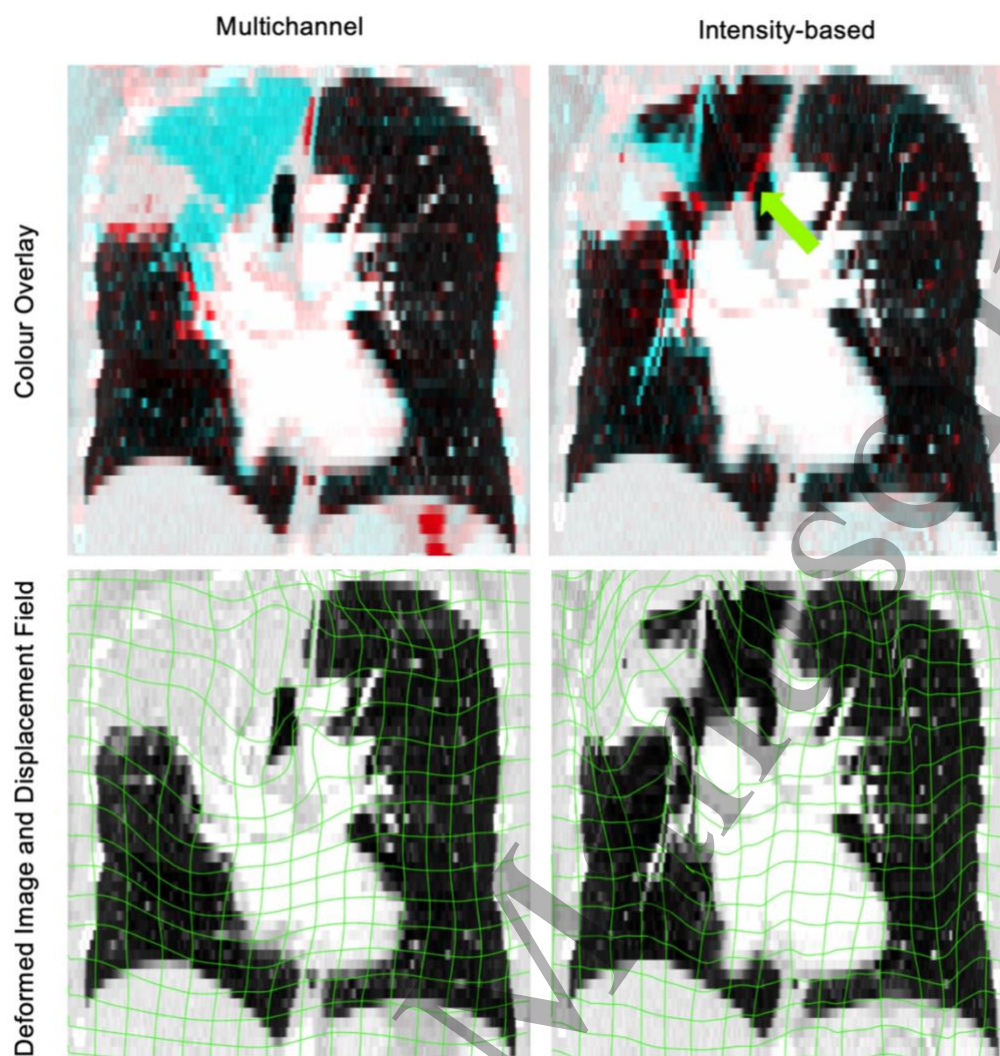
Fig. 8. Multichannel versus traditional intensity-based registration results for patient 15. The anatomically implausible deformations of the intensity approach are apparent in the bottom right image, where the displacement field of the registration is displayed over the registration result. The trachea in the deformed image has been stretched to the size of the upper right lobe in the baseline scan. The green arrow in the colour overlay (top right) points to the airway boundary of the baseline scan that has been stretched and is therefore missing from the deformed image. In comparison, the displacement field in the multichannel result is smooth, with no implausible or extreme deformations present.

1   **4.   Discussion**

2

3   Baseline and 12-month post-RT CT pairs from 15 patient datasets with RILD were split into four

4   categories according to expected registration difficulty and registered using the software NiftyReg.

5   Diffeomorphic feature-based registrations were performed where only salient features that were

6   consistent between the two images of a pair were used. These features included the lung boundaries,

7   main airways and vessels. The CT intensity information was disregarded in order to minimise the effect

8   of severe, non-deformable tissue damage on the registration results. The results were evaluated

9   quantitatively by calculation of the post-registration landmark distance at a number of manually

10   identified anatomical landmark pairs distributed across both lungs. Quantitative findings were critically

11   evaluated using visual inspection. We have demonstrated that our proposed method is suitable for

12   aligning pre-RT and follow-up CTs from lung cancer RT patients exhibiting considerable anatomical

13   changes due to RILD. This will facilitate future investigations into longitudinal changes to the local

14   parenchymal tissue occurring due to RILD, and to relate these to the RT dose that was delivered.

15

16   Improvement in image alignment was achieved for all patient datasets. Category 1 and 2 cases saw the

17   biggest improvements in alignment and the best overall results. Category 3 and 4 cases saw smaller

18   quantitative improvements in comparison, however visually notable improvements in alignment were

19   observed for all patients. Overall, good local alignment was achieved for all patients. The performance

20   of the registrations for other timepoints (3, 6, 24 month follow-up) was investigated for four patient

21   datasets. It was found that the landmark distances D_{reg} mostly increased over time, as is expected due

22   to more the extreme deformations of chronic RILD. The lowest registration errors for all patients were

23   measured when registering 3-month scans.

24

25   Results from the proposed multi-channel feature-based methodology were compared to results from a

26   traditional intensity-based DIR methodology. Our results indicate that for co-registration of serial CT

27   scans in the presence of RILD our novel method is superior to the traditional intensity-based approach.

28   The intensity-based registration achieved comparable results to our method for patients with modest

29   anatomical changes between baseline and 12 months but produced highly implausible results when the

30   damage was more pronounced.

31

32   Even though the intensity information of the CT is excluded from the registrations in order to minimise

33   the effects of the extensive tissue damage on the results, large geometric changes also occur in the

34   vasculature of the patients. For example, in atelectatic parts of the lung, vessels collapse under the

35   pressure of the surrounding tissue, making them unrecognisable in a CT. If a region of the lung is

36   damaged by radiation and is caused to shrink, consolidate or move, vessels supplying that region of the

37   lung will follow along. This means that there is not a perfect correspondence even between "consistent"

1   anatomical features when so much time has passed after radiotherapy. These geometric changes also
2   affect the main airways and lung boundaries but, in those cases, correspondence is considerably easier
3   to establish due to the larger scale and less repetitive nature of these structures compared to vessels.
4   This is why the lung boundaries and main airways are remarkably well aligned even in the most difficult
5   cases, but small-scale vessels and deeper airways can be misaligned. This also has a considerable impact
6   on our ability to accurately evaluate the accuracy of the registrations. Landmark pair identification is
7   already a challenging and laborious task but even more so in datasets that carry such extreme anatomical
8   changes between time points. In many cases, it is impossible to identify corresponding landmarks
9   between scans in some regions, which means that it is also impossible to quantitatively assess how
10 successful the registration is in those regions. Therefore, visual inspection of the registration results
11 thus becomes very important in challenging applications such as ours. Even so, it is not a perfect way
12 to completely capture all facets of the results.

13

14 Comparing our results with those achieved in other studies is informative but can also be misleading.
15 In the literature, even when the word "longitudinal" is used to describe the temporal distance between
16 scans, this usually means 3 months post-RT at most and even in these cases, patients with dramatic
17 geometric changes between time points, and especially atelectasis, are usually excluded. In the most
18 comparable piece of work by Guy et al. (2018), some level of atelectasis was present in all the scans.
19 In that study a mean (st. dev.) of 2.60 (0.90) mm landmark error was achieved, however, the scans were
20 only a few weeks apart, as mid-treatment scans were used. This means that geometric changes that
21 come with chronic RILD have not yet developed, making the registration process less complex.
22 Additionally, their mean landmark distance before DIR was 9.93mm whereas for our data it was
23 considerably higher at 15.95mm. In Cunliffe et al. (2015), mean errors of 2.5 mm and 4.6 mm were
24 found when registering pre-RT and 3-month post-RT CTs in the presence of damage by two different
25 DIR algorithms, namely Demons and Morphons. However, the analysis was carried out only in a
26 number of small regions across the lungs, and the PTV, a region that is hard to align and can give high
27 errors, was excluded. On the other hand, we tried to focus on landmarks around the tumour and areas
28 of RILD, as, although these are the regions that are hardest to align, they are also the ones of most
29 interest. In Spijkerman et al. (2014), the best performing, medium, and worst performing groups had
30 errors of 3.8 mm, 4.5 mm and 8.0 mm respectively. Once again, the temporal distance between scans
31 was only about 4 months. The EMPIRE10 challenge was a chest CT registration challenge held at
32 MICCAI 2010 (Murphy et al 2011). Some teams managed to obtain low landmark errors of < 1mm,
33 however, only 8 out of 30 scan pairs available were longitudinal (9-14 months between baseline and
34 follow-up scan) and no radiation damage was present, meaning that standard intensity-based approaches
35 could be successfully applied.

36

The mean landmark error for our 3-month registrations of 3.5mm might be a more appropriate comparison with the results in the literature, however, this number is only based on four datasets so further evaluation is needed. When taking into consideration that the scans used in our study include later follow-up time-point scans, display more pronounced anatomical and geometrical changes due to RILD, and that our evaluation deliberately tried to include more landmarks from the most challenging regions, we consider our results competitive to those presented in the literature. Furthermore, we expect that our approach would achieve better results than other published methods on scans from 6 months or later follow-up, that are of most interest when studying chronic effects of RILD.

This study was limited by the need for detailed manual editing of the lung segmentations as accurate automatic segmentations of this data were not available at the time of this study. Currently, we are developing an automatic lung segmentation that can successfully be applied to RILD datasets and we aim to utilise it for future studies once it has been validated. Lobe segmentations would have also been included if available as they would provide additional corresponding elements throughout the lungs. However, current lobe segmentation algorithms do not yet perform well on scans with severe damage, especially atelectasis, or on scans with large slice thicknesses such as some of those included in this study. An attempt at automatically generating them using the pulmonary lobe segmentation algorithm published by Xie et al. (2020) was unsuccessful when atelectasis was present in the scans.

In the future we intend to develop a fully automated pipeline for registrations. This will require methods to accurately and robustly segment the salient features without any manual intervention, possibly including additional structures such as lobe fissures and deeper airways. These automatic segmentation methods will need to be thoroughly validated, and the sensitivity of the registration results to the segmentation accuracy will be investigated and compared to the results presented in this paper. We will also explore the use of weakly supervised deep learning based registration approaches, that can take advantage of features and structures that have been delineated in the training data, but are not required when applying the trained network to new, unseen data.

5. Conclusion

In this work, we proposed a novel registration methodology tailored to co-register longitudinal CT scans in the presence of RILD. We have demonstrated that our method is able to successfully align 12-month follow up scans with pre-radiotherapy scans, even in the presence of large anatomical changes such as consolidation and atelectasis. The method was also shown to perform well on follow-up scans acquired at 3, 6, and 24 months after radiotherapy. The quality of the registration varies with the extent of anatomical and geometrical changes characteristic of RILD present in the scans. This work will facilitate future work studies aiming at better understanding the local parenchymal tissue changes caused by RILD, as well as provide insights into dose-response relationships.

24

1   REFERENCES

2

3   Choi, Y. W., Munden, R. F., Erasmus, J. J., Park, K. J., Chung, W. K., Jeon, S. C., &

4   Park, C. K. (2004). Effects of radiation therapy on the lung: Radiologic appearances and

5   differential diagnosis. In *Radiographics* (Vol. 24, Issue 4, pp. 985–997). Radiological

6   Society of North America Inc. https://doi.org/10.1148/rg.244035160

7   Cunliffe, A. R., White, B., Justusson, J., Straus, C., Malik, R., Al-Hallaq, H. A., &

8   Armato, S. G. (2015). Comparison of Two Deformable Registration Algorithms in the

9   Presence of Radiologic Change Between Serial Lung CT Scans. *Journal of Digital*

10   *Imaging*, *28*(6), 755–760. https://doi.org/10.1007/s10278-015-9789-1

11   Doel, T. (2012). Developing Clinical Measures of Lung Function in COPD Patients

12   Using Medical Imaging and Computational Modelling. PhD thesis. Oxford University,

13   UK

14   Fan, M., Marks, L. B., Lind, P., Hollis, D., Woel, R. T., Bentel, G. G., Anscher, M. S.,

15   Shafman, T. D., Coleman, R. E., Jaszczak, R. J., & Munley, M. T. (2001). Relating

16   radiation-induced regional lung injury to changes in pulmonary function tests.

17   *International Journal of Radiation Oncology Biology Physics*, *51*(2), 311–317.

18   https://doi.org/10.1016/S0360-3016(01)01619-4

19   Frangi, A. F., Niessen, W. J., Vincken, K. L., & Viergever, M. A. (1998). Multiscale

20   vessel enhancement filtering. *Lecture Notes in Computer Science (Including Subseries*

21   *Lecture Notes in Artificial Intelligence and Lecture Notes in Bioinformatics)*, *1496*, 130–

22   137. https://doi.org/10.1007/bfb0056195

23   Fu, Y., Brown, N. M., Saeed, S. U., Casamitjana, A., Baum, Z. M. C., Delaunay, R.,

24   Yang, Q., Grimwood, A., Min, Z., Blumberg, S. B., Iglesias, J. E., Barratt, D. C.,

25   Bonmati, E., Alexander, D. C., Clarkson, M. J., Vercauteren, T., & Hu, Y. (2020).

26   DeepReg: A deep learning toolkit for medical image registration. In *arXiv* (Vol. 5, Issue

27   55, p. 2705). arXiv. https://doi.org/10.21105/joss.02705

28   Guy, C. L., Weiss, E., Christensen, G. E., Jan, N., & Hugo, G. D. (2018). CALIPER: A

29   deformable image registration algorithm for large geometric changes during radiotherapy

1   for locally advanced non-small cell lung cancer. *Medical Physics*, *45*(6), 2498–2508.

2   https://doi.org/10.1002/mp.12891

3   Howlader, N., Forjaz, G., Mooradian, M. J., Meza, R., Kong, C. Y., Cronin, K. A.,

4   Mariotto, A. B., Lowy, D. R., & Feuer, E. J. (2020). The Effect of Advances in Lung-

5   Cancer Treatment on Population Mortality. *New England Journal of Medicine*, *383*(7),

6   640–649. https://doi.org/10.1056/nejmoa1916623

7   Ikezoe, J., Takashima, S., Morimoto, S., Kadowaki, K., Takeuchi, N., Yamamoto, T.,

8   Nakanishi, K., Isaza, M., Arisawa, J., Ikeda, H., Masaki, N., & Kozuka, T. (1988). CT

9   appearance of acute radiation-induced injury in the lung. *American Journal of*

10   *Roentgenology*, *150*(4), 765–770. https://doi.org/10.2214/ajr.150.4.765

11   Landau, D. B., Hughes, L., Baker, A., Bates, A. T., Bayne, M. C., Counsell, N., Garcia-

12   Alonso, A., Harden, S. V., Hicks, J. D., Hughes, S. R., Illsley, M. C., Khan, I., Laurence,

13   V., Malik, Z., Mayles, H., Mayles, W. P. M., Miles, E., Mohammed, N., Ngai, Y., …

14   Fenwick, J. D. (2016). IDEAL-CRT: A Phase 1/2 Trial of Isotoxic Dose-Escalated

15   Radiation Therapy and Concurrent Chemotherapy in Patients With Stage II/III Non-Small

16   Cell Lung Cancer. *International Journal of Radiation Oncology Biology Physics*, *95*(5),

17   1367–1377. https://doi.org/10.1016/j.ijrobp.2016.03.031

18   Lopez Guerra, J. L., Gomez, D. R., Zhuang, Y., Levy, L. B., Eapen, G., Liu, H., Mohan,

19   R., Komaki, R., Cox, J. D., & Liao, Z. (2012). Changes in pulmonary function after three-

20   dimensional conformal radiotherapy, intensity-modulated radiotherapy, or proton beam

21   therapy for non-small-cell lung cancer. *International Journal of Radiation Oncology*

22   *Biology Physics*, *83*(4), e537–e543. https://doi.org/10.1016/j.ijrobp.2012.01.019

23   Ma, J., Zhang, J., Zhou, S., Hubbs, J. L., Foltz, R. J., Hollis, D. R., Light, K. L., Wong, T.

24   Z., Kelsey, C. R., & Marks, L. B. (2009). Association Between RT-Induced Changes in

25   Lung Tissue Density and Global Lung Function. *International Journal of Radiation*

26   *Oncology Biology Physics*, *74*(3), 781–789. https://doi.org/10.1016/j.ijrobp.2008.08.053

27   Marks, L. B., Fan, M., Clough, R., Munley, M., Bentel, G., Coleman, R. E., Jaszczak, R.,

28   Hollis, D., & Anscher, M. (2000). Radiation-induced pulmonary injury: Symptomatic

29   versus subclinical endpoints. *International Journal of Radiation Biology*, *76*(4), 469–475.

30   https://doi.org/10.1080/095530000138466

1 Mehta, V. (2005). Radiation pneumonitis and pulmonary fibrosis in non-small-cell lung

2 cancer: Pulmonary function, prediction, and prevention. *International Journal of*

3 *Radiation Oncology Biology Physics*, *63*(1), 5–24.

4 https://doi.org/10.1016/j.ijrobp.2005.03.047

5 Modat, M., Ridgway, G. R., Taylor, Z. A., Lehmann, M., Barnes, J., Hawkes, D. J., Fox,

6 N. C., & Ourselin, S. (2010). Fast free-form deformation using graphics processing units.

7 *Computer Methods and Programs in Biomedicine*, *98*(3), 278–284.

8 https://doi.org/10.1016/j.cmpb.2009.09.002

9 Modat, M., Daga, P., Cardoso, M. J., Ourselin, S., Ridgway, G. R., & Ashburner, J.

10 (2012). Parametric non-rigid registration using a stationary velocity field. *Proceedings of*

11 *the Workshop on Mathematical Methods in Biomedical Image Analysis*, 145–150.

12 https://doi.org/10.1109/MMBIA.2012.6164745

13 Murphy, K., Van Ginneken, B., Reinhardt, J. M., Kabus, S., Ding, K., Deng, X., Cao, K.,

14 Du, K., Christensen, G. E., Garcia, V., Vercauteren, T., Ayache, N., Commowick, O.,

15 Malandain, G., Glocker, B., Paragios, N., Navab, N., Gorbunova, V., Sporring, J., …

16 Pluim, J. P. W. (2011). Evaluation of registration methods on thoracic CT: The

17 EMPIRE10 challenge. *IEEE Transactions on Medical Imaging*, *30*(11), 1901–1920.

18 https://doi.org/10.1109/TMI.2011.2158349

19 Ourselin, S., Roche, A., Subsol, G., Pennec, X. & Ayache, N. (2001) Reconstructing a 3D

20 structure from serial histological sections *Image Vis. Comput.* **19** 25–31.

21 Rosen, I. I., Fischer, T. A., Antolak, J. A., Starkschall, G., Travis, E. L., Tucker, S. L.,

22 Hogstrom, K. R., Cox, J. D., & Komaki, R. (2001). Correlation between lung fibrosis and

23 radiation therapy dose after concurrent radiation therapy and chemotherapy for limited

24 small cell lung cancer. *Radiology*, *221*(3), 614–622.

25 https://doi.org/10.1148/radiol.2213992043

26 Simone, C. B. (2017). Thoracic Radiation Normal Tissue Injury. In *Seminars in*

27 *Radiation Oncology* (Vol. 27, Issue 4, pp. 370–377). W.B. Saunders.

28 https://doi.org/10.1016/j.semradonc.2017.04.009

1   Spijkerman, J., Fontanarosa, D., Das, M., & Elmpt, W. (2014). Validation of nonrigid

2   registration in pretreatment and follow-up PET/CT scans for quantification of tumor

3   residue in lung cancer patients. *Journal of Applied Clinical Medical Physics*, *15*(4), 240–

4   250. https://doi.org/10.1120/jacmp.v15i4.4847

5   Thirion, J.-P., & Thirion, J.-P. (1998). Image matching as a diffusion process: an analogy

6   with Maxwell's demons. In *Medical Image Analysis* (Vol. 2, Issue 3). Elsevier.

7   https://hal.inria.fr/inria-00615088

8   Veiga, C., Chandy, E., Jacob, J., Yip, N., Szmul, A., Landau, D., & McClelland, J. R.

9   (2020). Investigation of the evolution of radiation-induced lung damage using serial CT

10 imaging and pulmonary function tests. *Radiotherapy and Oncology*, *148*, 89–96.

11 https://doi.org/10.1016/j.radonc.2020.03.026

12 Veiga, C., Jacob, J., Yip, N., Szmul, A., Landau, D., & McClelland, J. (2019). Objective

13 imaging biomarkers to quantify the evolution of radiation-induced lung

14 damage.   *In: Proceedings of the 19th International Conference on the Use of*

15 *Computers in Radiation Therapy.   ICCR (2019)   (In Press).* . http://iccr-mcma.org/

16 Veiga, C., Landau, D., Devaraj, A., Doel, T., Hawkes, D., & McClelland, J. (2017).

17 Quantification of Radiation Therapy-Induced Diaphragmatic Changes Using Serial CT

18 Imaging. *International Journal of Radiation Oncology*Biology*Physics*, *99*(2), S12.

19 https://doi.org/10.1016/j.ijrobp.2017.06.045

20 Veiga, C., Landau, D., McClelland, J. R., Ledermann, J. A., Hawkes, D., Janes, S. M., &

21 Devaraj, A. (2018). Long term radiological features of radiation-induced lung damage.

22 *Radiotherapy and Oncology*, *126*(2), 300–306.

23 https://doi.org/10.1016/j.radonc.2017.11.003

24 Veiga, C., Mcclelland, J. R., Landau, D., Devaraj, A., Hawkes, D., & Mcclelland, J. R.

25 (2016). *Challenges in the registration of serial CT images from lung radiotherapy*

26 *patients Image-guided and adaptive radiotherapy View project ADSCaN View project*

27 *Challenges in the registration of serial CT images from lung radiotherapy patients*.

28 http://cmic.cs.ucl.ac.uk/home/software/

1 Vercauteren, T., Pennec, X., Perchant, A., & Ayache, N. (2009). Diffeomorphic demons:

2 efficient non-parametric image registration. *NeuroImage*, *45*(1 Suppl).

3 https://doi.org/10.1016/j.neuroimage.2008.10.040

4 Wrangsjö, A., Pettersson, J., & Knutsson, H. (2005). Non-rigid registration using

5 Morphons. *Lecture Notes in Computer Science*, *3540*, 501–510.

6 https://doi.org/10.1007/11499145_51

7 Xie, W., Jacobs, C., Charbonnier, J. P., & Van Ginneken, B. (2020). Relational Modeling

8 for Robust and Efficient Pulmonary Lobe Segmentation in CT Scans. *IEEE Transactions*

9 *on Medical Imaging*, *39*(8), 2664–2675. https://doi.org/10.1109/TMI.2020.2995108

10 Yushkevich, P. A., Piven, J., Hazlett, H. C., Smith, R. G., Ho, S., Gee, J. C., & Gerig,

11 G.   (2006). User-guided 3D active contour segmentation of anatomical structures:

12 Significantly improved efficiency and reliability. *NeuroImage, 31*(3), 1116–1128.

13 https://doi.org/10.1016/j.neuroimage.2006.01.015

14

15